Atmospheric Frontogenesis: A Numerical Experiment

R. T. WILLIAMS[1]

Massachusetts Institute of Technology, Cambridge

(Manuscript received 9 March 1967)

ABSTRACT

The objective of this study is to produce a narrow frontal zone from a field which initially contains only large-scale variations. In the model, all quantities except the temperature and pressure are independent of y (latitude), and these have y derivatives which are only functions of z. The hydrostatic Boussinesq equations are employed, and friction, heating, and the variation of f are neglected. In the experiment a growing baroclinic wave distorts itself in such a way that a cold frontal zone is produced. Comparative integrations with two different values of Δx indicate that the front would become discontinuous within a finite period of time if Δx were made arbitrarily small.

A crude analytical solution is obtained which has the main characteristics of the numerical solutions. Mathematically, the analytical solution is similar to those which describe the formation of shocks and pressure jumps. Physically, the frontal case is quite different because the vorticity is always much larger than the divergence.

1. Introduction

The existence of atmospheric fronts has been recognized for many years. However, no adequate mathematical theory is available which can explain their formation. The problem is essentially one of producing a small-scale motion field from one which initially contains only large scales of motion. This energy cascade is necessary because the principal source of disturbance energy is baroclinic instability which occurs on scales of 1000 km or more, and because frontal zones have scales of 100 km or less. Also, the time scale for the frontogenesis process must be small since fronts often form in less than 24 hr.

Bergeron (1928) and others have attributed frontogenesis to nondivergent horizontal fields of deformation. This process should be described by the quasi-geostrophic equations. However, these deformation fields cannot produce a real front from large-scale initial conditions. In order to show this, we consider the geostrophic potential vorticity in the following form which was derived by Charney and Stern (1962):

$$q=\nabla^2\psi+\frac{f}{\rho_s}\frac{\partial}{\partial z}\left[\left(\rho_s\Big/\frac{d(\ln\theta_s)}{dz}\right)\ln\left(\frac{\theta}{\theta_s}\right)\right]+\beta y. \quad (1.1)$$

Here ψ is the geostrophic stream function, and ρ_s and θ_s are obtained from a standard atmosphere. The other symbols have their usual meaning. This quantity is conserved by the quasi-geostrophic equations so that if q is small initially, it must remain small. The first term in q, which is the relative vorticity, will be a large positive quantity at a true front. Since ρ_s and θ_s are slowly varying functions of z, the only way that the second term can become large and negative is for $\partial\theta/\partial z$ to be negative. This is not possible because the atmosphere must be statically stable. Thus, at a true front, the geostrophic potential vorticity will be very large and, therefore, this state could not have evolved from a state where q was everywhere small. This means that the quasi-geostrophic equations cannot produce a true front from large-scale initial conditions. However, Stone (1966) has shown that quasi-geostrophic equations can produce a pseudo front when a deformation field is present. In his solution the temperature gradient grows exponentially in time at the surface, but it reaches a finite value in the interior. The front does not tilt with height and the vorticity at the front is zero. A true front does not have the latter two features.

Eliassen (1959) proposed a mechanism which depends on the latent heat of condensation in the frictionally driven vertical motion at the front. However, intense atmospheric fronts are observed which are nearly free of condensation. Also, fronts occur in the ocean (Knauss, 1957) and in some dishpan experiments (Faller, 1956). Although condensation may be important in certain circumstances, it cannot be essential in frontogenesis.

If we permit the influence of vertical deformation fields in our equations, we can eliminate the constraint which arises from the quasi-geostrophic approximation. This requires that the divergent part of the wind be included in the advective terms in the equations. The importance of the divergent component of the advection is proportional to the Rossby number [$\mathrm{Ro}=V/f\ell$, where V is the velocity scale and ℓ the space scale; see Charney (1962) and Phillips (1963)]. For large-scale flow, Ro is normally small and the quasi-geostrophic

[1] Present affiliation: Department of Meteorology, University of Utah, Salt Lake City.

Unauthenticated | Downloaded 10/14/24 09:06 AM UTC

equations are accurate. In order for the divergent effects to become important, the quasi-geostrophic equation must force Ro to increase. This can occur if ℓ decreases as it does in Stone's solution or if V increases as it does during baroclinic instability. In this paper we will employ the latter procedure to force Ro up sufficiently to make the divergent horizontal advection important. We shall see that in this case the vertical deformation fields produce a realistic front within a reasonable length of time. This process has been investigated numerically by Arakawa (1962), Edelmann (1963) and Williams (1965).

The balance equations consist of the zero- and first-order terms in the Rossby number from the vorticity and divergence equations plus the complete first law of thermodynamics (Charney, 1962). The balance equations allow for the effect of divergence in the vertical deformation fields, but they are not convenient for numerical solution. Thus, we shall employ the hydrostatic primitive equations because they are easier to solve and because they are more general. The balance equations will prove useful in interpreting our numerical solutions.

In Section 2, the Boussinesq equations are given and the modeling relations are introduced. In the model the time-dependent quantities are functions of x and z only. The x-averaged temperature and pressure have linear variations in the y direction and f is assumed to be constant. The finite difference approximations are found in Section 3. A scale analysis is presented in Section 4 which is useful in the discussion of the numerical solutions. The initial conditions are given in Section 5 and the numerical solutions are presented and discussed in Section 6. The initial state consists of a small-amplitude sinusoidal disturbance which is superimposed upon an unstable baroclinic current. When the disturbance amplitude becomes large, the sine wave is distorted in such a way that a frontal zone is formed. In Section 7 a crude analytical model is presented which reproduces some of the characteristics of the numerical solutions. In Section 8 conclusions and suggestions for further work are given.

2. Basic equations

In this study we employ the Boussinesq equations, and we bound our domain with two rigid horizontal planes. The compressibility of the atmosphere, which is neglected in the Boussinesq approximation, should not be of qualitative importance since the density scale height in the atmosphere is much larger than the thickness of typical frontal zones. The replacement of the tropopause by a rigid horizontal surface can be expected to give large errors in that region, but the resulting errors near the lower boundary should be small. We shall see that these approximations will permit us to find solutions which have a type of vertical symmetry. The hydrostatic approximation is also used in this study and it should be good throughout the frontogenesis process since the horizontal scale should remain much larger than the vertical scale (Lamb, 1945, p. 258).

The Boussinesq equations which were obtained by Ogura and Phillips (1962) can be written in the following form when the earth's rotation is included:

$$\frac{\partial \mathbf{V}}{\partial t}+\nabla\cdot(\mathbf{V}\mathbf{V})+\frac{\partial}{\partial z}(w\mathbf{V})+\nabla\phi+f\mathbf{k}\times\mathbf{V}=0, \tag{2.1}$$

$$\frac{\partial \theta}{\partial t}+\nabla\cdot\theta\mathbf{V}+\frac{\partial(w\theta)}{\partial z}=0, \tag{2.2}$$

$$\nabla\cdot\mathbf{V}+\frac{\partial w}{\partial z}=0, \tag{2.3}$$

$$\frac{\partial \phi}{\partial z}=\frac{g\theta}{\theta_0}, \tag{2.4}$$

where:

θ_0 = constant reference potential temperature,
P_0 = constant reference pressure,
$\kappa = R/C_p$,
$\theta = T(P_0/P)^\kappa - \theta_0$ = departure of the potential temperature from θ_0, and
$\phi = C_p\theta_0(P/P_0)^\kappa + gz$.

Heating and friction have been neglected in these equations even though they may be important under certain conditions.

In our model, only ϕ and θ are allowed to have a variation with latitude and this variation is linear and independent of longitude and time. All other dependent variables are not functions of the latitude. We assume that f is constant, and we introduce a Cartesian coordinate system with x increasing toward the east and y increasing toward the north. The x and y velocity components are u and v, respectively.

For this model, Eqs. (2.1)–(2.3) can be written in the following form:

$$\frac{\partial u}{\partial t}+\frac{\partial(uu)}{\partial x}+\frac{\partial(wu)}{\partial z}+\frac{\partial \phi}{\partial x}-fv=0, \tag{2.5}$$

$$\frac{\partial v}{\partial t}+\frac{\partial(uv)}{\partial x}+\frac{\partial(wv)}{\partial z}+\frac{\partial \phi}{\partial y}+fu=0, \tag{2.6}$$

$$\frac{\partial \theta}{\partial t}+\frac{\partial(u\theta)}{\partial x}+\frac{\partial(w\theta)}{\partial z}+v\frac{\partial \theta}{\partial y}=0, \tag{2.7}$$

$$\frac{\partial u}{\partial x}+\frac{\partial w}{\partial z}=0. \tag{2.8}$$

Unauthenticated | Downloaded 10/14/24 09:06 AM UTC

Note that $\partial\phi/\partial y=\partial\bar{\phi}/\partial y$, where the bar indicates the x average. In this paper we take

$$\partial\theta/\partial y=\text{constant}. \tag{2.9}$$

The boundary conditions are

$$w=0, \quad z=0, D, \tag{2.10}$$

where D is the distance between the horizontal plates.

The integral of Eq. (2.4) gives the departure of ϕ from its vertical average, and this average can be obtained as follows. We define the averages

$$\bar{(\ )}\equiv\frac{1}{2\pi L}\int_0^{2\pi L}(\ )dx, \quad \langle(\ )\rangle_{\text{av}}\equiv\frac{1}{D}\int_0^{D}(\ )dz, \tag{2.11}$$

where $2\pi L$ is the periodicity of the fields in x. If we average Eq. (2.8) vertically and employ (2.10) we obtain

$$\frac{\partial\langle u\rangle_{\text{av}}}{\partial x}=0 \quad \text{or} \quad \langle u\rangle_{\text{av}}=\overline{\langle u\rangle_{\text{av}}}. \tag{2.12}$$

Similarly, the vertical average of (2.5) is

$$\frac{\partial\langle u\rangle_{\text{av}}}{\partial t}+\frac{\partial\langle(uu)\rangle_{\text{av}}}{\partial x}+\frac{\partial\langle\phi\rangle_{\text{av}}}{\partial x}-f\langle v\rangle_{\text{av}}=0. \tag{2.13}$$

If this equation is in turn averaged with x and if periodicity in x is imposed, we obtain

$$\frac{d\langle(\bar{u})\rangle_{\text{av}}}{dt}-f\langle(\bar{v})\rangle_{\text{av}}=0. \tag{2.14}$$

The quantity $\langle(\bar{v})\rangle_{\text{av}}$ represents the net mass flux in the latitudinal direction. If $\langle(\bar{v})\rangle_{\text{av}}$ were different from zero, $\langle(\partial\bar{w}/\partial z)\rangle_{\text{av}}$ could not be zero if a wall were present at some value of y. Since this would violate the boundary conditions [Eq. (2.10)], we shall require that

$$\langle(\bar{v})\rangle_{\text{av}}=0. \tag{2.15}$$

If we use relations (2.12)–(2.15), we obtain

$$\frac{\partial\langle\phi\rangle_{\text{av}}}{\partial x}=-\frac{\partial\langle(uu)\rangle_{\text{av}}}{\partial x}+f\langle v\rangle_{\text{av}}. \tag{2.16}$$

The corresponding equation for $\partial\langle\phi\rangle_{\text{av}}/\partial y$ is obtained by averaging Eq. (2.6) in x and z and by introducing (2.15), i.e.,

$$\frac{\partial\langle\phi\rangle_{\text{av}}}{\partial y}=-f\langle(\bar{u})\rangle_{\text{av}}. \tag{2.17}$$

Eqs. (2.14), (2.15) and (2.17) show that the x- and z-averaged zonal wind is geostrophic and independent of time. If we use (2.4), (2.9), (2.16) and (2.17), we can rewrite (2.5) and (2.6) in the forms

$$\frac{\partial u}{\partial t}+\frac{\partial(uu)}{\partial x}-\frac{\partial\langle(uu)\rangle_{\text{av}}}{\partial x}+\frac{\partial(wu)}{\partial z}-f(v-\langle v\rangle_{\text{av}})+\frac{\partial}{\partial x}(\phi-\langle\phi\rangle_{\text{av}})=0, \tag{2.18}$$

$$\frac{\partial v}{\partial t}+\frac{\partial(uv)}{\partial x}+\frac{\partial(wv)}{\partial z}+f(u-\langle u\rangle_{\text{av}})+\frac{g}{\theta_0}\frac{\partial\theta}{\partial y}(z-D/2)=0. \tag{2.19}$$

If we integrate the hydrostatic equation (2.4) and remove the vertical mean, we obtain

$$\phi-\langle\phi\rangle_{\text{av}}=\frac{g}{\theta_0}\left[\int_0^z\theta dz-\left\langle\int_0^z\theta dz\right\rangle_{\text{av}}\right]. \tag{2.20}$$

The following energy integral is an invariant for this model:

$$E=[\langle(\overline{u^2})\rangle_{\text{av}}+\langle(\overline{v^2})\rangle_{\text{av}}]/2-g\langle(\overline{z\theta/\theta_0})\rangle_{\text{av}}. \tag{2.21}$$

We will use this property of the continuous equations in estimating the error in the numerical solutions which will be presented later.

3. Finite difference approximations

We shall solve Eqs. (2.7), (2.8), (2.18), (2.19) and (2.20) numerically by introducing finite differences in x, z and t. The solutions are obtained by a simple marching process, but if the horizontal variations were two-dimensional, Poisson's equation would have to be solved at each time step (Smagorinsky, 1958; Hinkelmann, 1959).

The vertical domain is divided into $2K$ layers, not necessarily of equal thickness, and the surfaces separating the layers are denoted by k. The arrangement of variables on the bounding surfaces is shown in Fig. 1. The divergence of the vertical flux of the scalar S at $z=z_k$ is approximated as

$$\left[\frac{\partial(wS)}{\partial z}\right]_k=\frac{w_{k+\frac{1}{2}}(S_{k+1}+S_k)-w_{k-\frac{1}{2}}(S_k+S_{k-1})}{2(z_{k+\frac{1}{2}}-z_{k-\frac{1}{2}})}. \tag{3.1}$$

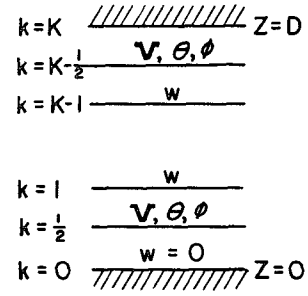

FIG. 1. Arrangement of variables in z.

Unauthenticated | Downloaded 10/14/24 09:06 AM UTC

The finite difference approximation to the integral in Eq. (2.20) is

$$\int_0^{z_k}\theta dz=\sum_{j=\frac{1}{2}}^{j=k-1}\left[\frac{(\theta_{j+1}+\theta_j)}{2}(z_{j+1}-z_j)\right]+C,\quad k>\tfrac{1}{2}. \tag{3.2}$$

The value of $C=\int_0^{z1/2}\theta dz$ is immaterial since it will disappear when the vertical average is removed. The finite difference integral of Eq. (2.8) is

$$w_k=-\sum_{j=\frac{1}{2}}^{j=k-\frac{1}{2}}\left[\frac{\partial u_j}{\partial x}(z_{j+\frac{1}{2}}-z_{j-\frac{1}{2}})\right]. \tag{3.3}$$

The vertical grid structure was introduced by Lorenz (1960) for use in the balance equations.

All of the dependent variables occur at each x grid point. The x derivatives are approximated as

$$\left(\frac{\partial S}{\partial x}\right)_i=\frac{S_{i+1}-S_{i-1}}{2\Delta x}, \tag{3.4}$$

$$\left[\frac{\partial(uS)}{\partial x}\right]_i=\frac{(u_{i+1}+u_i)(S_{i+1}+S_i)-(u_i+u_{i-1})(S_i+S_{i-1})}{4\Delta x}. \tag{3.5}$$

Here i denotes the grid index and Δx the mesh length. This is a variant of the finite difference scheme that Arakawa (1966) developed [see also Lilly (1965)]. The Arakawa scheme is designed to avoid the nonlinear computational instability which was discovered by Phillips (1959). In particular, the finite difference approximation to the integral,

$$I\equiv\left\langle\left(\overline{\frac{S\partial(uS)}{\partial x}}\right)\right\rangle_{\text{av}}+\left\langle\left(\overline{\frac{S\partial(wS)}{\partial z}}\right)\right\rangle_{\text{av}}, \tag{3.6}$$

is zero when (3.1) and (3.5) are used. The integral I is always zero in the continuous case. If the domain averages of u^2, v^2 and θ^2 are conserved by the nonlinear terms throughout a numerical integration, than no nonlinear computational instability can occur. When finite differences in time are employed, these quantities will not be identically conserved and instability may arise.

The continuous equations conserve the total energy E, which is given by Eq. (2.21). If nonlinear computational instability occurs, E cannot be conserved. We shall see that E remains nearly constant in our numerical solutions, which indicates that the spurious computational production of energy is small. This is important because we do not want our computational scheme to introduce a small-scale energy source which could produce a false front.

Centered time differences are used throughout this study with the exception of the first time step which is forward.

4. Scale analysis

In this section we present a scale analysis which will be very useful when we analyze the numerical solutions of Section 6. We begin by defining the following new independent variables:

$$x^*=x/l,\quad z^*=z/d,\quad t^*=(U/l)t. \tag{4.1}$$

Here ℓ and d are the horizontal and vertical scales near the front and $U=-(gD/2f\theta_0)(\partial\theta/\partial y)$ is one-half the total variation in the zonal geostrophic wind [see Eq. (2.19)]. The dependent variables are broken up and scaled by the relations

$$\left.\begin{aligned}u&=U(2az^*-1)+\text{Ro}Vu^*\\ v&=Vv^*\\ w&=(\text{Ro}Vd/l)w^*\\ \theta&=\bar\theta_I+(\theta_0flV/gd)\theta^*\\ \phi&=-(g/\theta_0)\int\bar\theta_I dz+fVl\phi^*\end{aligned}\right\}. \tag{4.2}$$

We set $\langle(\bar u)\rangle_{\text{av}}$ equal to zero since it is an arbitrary constant. The scaling for the meridional component of the wind is V, and V is thus a measure of the disturbance amplitude. The initial theta field is θ_I. The dimensionless numbers which will appear in our analysis are

$$\text{Ro}=\frac{U}{fL},\quad \mathcal{R}\text{o}=\frac{V}{fl},\quad \Gamma=\frac{g}{\theta_0}\frac{d^2}{f^2l^2}\frac{d\bar\theta_I}{dz},$$
$$a=d/D,\quad b=l/L. \tag{4.3}$$

The horizontal and vertical scales of the initial disturbance are L and D. Ro is a Rossby number which is based on the geostrophic zonal wind and on the initial disturbance scale. $\mathcal{R}$o is the disturbance Rossby number, and, unlike Ro, it will vary in time. Γ is an inverse rotational Froude number which may be written $\Gamma=\mathcal{R}\text{o}^2\text{Ri}$ (Ri a Richardson number). The ratios of the disturbance scales to their initial values are given by a and b.

When the relations (4.1)–(4.3) are introduced in Eqs. (2.4), (2.5), (2.6), (2.7) and (2.8) they become:

$$\frac{\partial v^*}{\partial t^*}+(2az^*-1)\frac{\partial v^*}{\partial x^*}+bu^*+b\mathcal{R}\text{o}\left[u^*\frac{\partial v^*}{\partial x^*}+w^*\frac{\partial v^*}{\partial z^*}\right]=0, \tag{4.4}$$

$$-v^*+\frac{\partial\phi^*}{\partial x^*}+\frac{\text{Ro}^2\Gamma}{b}\left[\frac{\partial u^*}{\partial t^*}+(2az^*-1)\frac{\partial u^*}{\partial x^*}+2aw^*+b\mathcal{R}\text{o}\left(u^*\frac{\partial u^*}{\partial x^*}+w^*\frac{\partial u^*}{\partial z^*}\right)\right]=0, \tag{4.5}$$

Unauthenticated | Downloaded 10/14/24 09:06 AM UTC

$$\frac{\partial\theta^*}{\partial t^*}+(2az^*-1)\frac{\partial\theta^*}{\partial x^*}-2av^*+b\Gamma w^* +b\mathcal{R}o\left[u^*\frac{\partial\theta^*}{\partial x^*}+w^*\frac{\partial\theta^*}{\partial z^*}\right]=0, \quad (4.6)$$

$$\frac{\partial u^*}{\partial x^*}+\frac{\partial w^*}{\partial z^*}=0, \quad (4.7)$$

$$\frac{\partial\phi^*}{\partial z^*}-\theta^*=0. \quad (4.8)$$

The boundary conditions (2.10) are now

$$w^*=0, \quad z^*=0, a^{-1}. \quad (4.9)$$

This complicated non-dimensionalization is used so that the entire evolution of the disturbance can be described. This scaling is consistent with the numerical solutions.

5. Initial conditions

In this model the poleward temperature gradient $(\partial\theta/\partial y)$ is strictly constant. Also, we choose

$$\langle(\bar{u})\rangle_{\text{av}}=-(1/f)\partial\langle(\bar{\phi})\rangle_{\text{av}}/\partial y=0. \quad (5.1)$$

As a result, the geostrophic zonal wind increases linearly from $-U$ and the lower boundary to $+U$ at the upper boundary $[U-=(gD/2f\theta_0)(\partial\theta/\partial y)]$. Initially, we set the x-averaged zonal wind equal to the geostrophic zonal wind. The initial x-averaged stability $(\partial\bar{\theta}/\partial z)$ is independent of z. We superimpose upon this basic state a small amplitude wave which is sinusoidal in x.

The initial fields are given by the equations,

$$u=[(D/2)-z](g/f\theta_0)(\partial\theta/\partial y)+(ADg/(f^2\theta_0L)](\partial\theta/\partial y) \times\{[\alpha n^2\sinh Z-(Z/\alpha)(1-(\alpha/2)\coth(\alpha/2))\cosh Z] \times\cos(x/L)+n[\{(\alpha/2)\coth(\alpha/2)-1\} \times\cosh Z-Z\sinh Z]\sin(x/L)\}, \quad (5.2)$$

$$v=A\{n\alpha\sinh Z\cos(x/L)-[1-(\alpha/2)\coth(\alpha/2)] \times\cosh Z\sin(x/L)\}, \quad (5.3)$$

$$\theta=(z-D/2)(\partial\bar{\theta}_I/\partial z)-\theta_0f\alpha LA/(gD) \times\{-[1-(\alpha/2)\coth(\alpha/2)] \times\sinh Z\cos(x/L)-n\alpha\cosh Z\sin(x/L)\}, \quad (5.4)$$

where $1/\alpha=(Lf/D)[\theta_0/(g\partial\bar{\theta}_I/\partial z)]^{\frac{1}{2}}$, $Z=\alpha[(z/D)-\frac{1}{2}]$, and $n^2\alpha^2=[(\alpha/2)-\tanh(\alpha/2)][\coth(\alpha/2)-\alpha/2]$, A being the initial disturbance amplitude. The reason for choosing this particular initial disturbance will be given in Section 6.

The constants which define the initial state have the following numerical values:

$$A=3\text{ m sec}^{-1}, \qquad D=9\text{ km},$$
$$f=10^{-4}\text{ sec}^{-1}, \qquad g/\theta_0=0.0327\text{ m sec}^{-2}(^\circ\text{K})^{-1},$$
$$\frac{\partial\theta}{\partial y}=-10^{-5}\text{K m}^{-1}, \quad \partial\bar{\theta}_I/\partial z=3.9\text{K km}^{-1}. \quad (5.5)$$

The wavelength of the disturbance, $2\pi L$, is equal to 4000 km.

After finite differences are introduced, it is necessary to adjust the values of u which are given by (5.2) in order that

$$w_K=-\sum_{j=\frac{1}{2}}^{j=K-\frac{1}{2}}\frac{\partial u_j}{\partial x}(z_{j+\frac{1}{2}}-z_{j-\frac{1}{2}})=0. \quad (5.6)$$

This merely states that the finite difference vertical velocity at the upper boundary must be zero.

The initial fields given above have the odd symmetry property that

$$S(x, z-D/2)=-S(-x, -z+D/2), \quad (5.7)$$

where S is u, v, w or θ. It can be seen from the forecast equations that this symmetry property will be perpetuated. This symmetry could not be maintained if the compressibility of the atmosphere were considered or if f were allowed to vary with latitude.

The initial v field is shown as a function of x and z in Fig. 2a and the initial $\theta'=\theta-\bar{\theta}$ field in Fig. 2b. The symmetry noted above is clearly present in both fields.

6. Numerical solutions

Numerical solutions for a model which is similar to this one were given by Williams (1965). For simplicity, we shall refer to this paper as W2L. In this paper, two levels were employed and pressure was used as a vertical coordinate. Also, dp/dt was neglected at the lower boundary. The equations used in W2L correspond to those of the present model when $K=2$ except for changes in certain constants.

In W2L fairly realistic frontal zones were obtained as long as the horizontal scale was not too small. It is not surprising that the 2-level model would fail when the horizontal scale becomes small, because intense frontal zones have vertical structures which are too complicated to be described by only two levels. In this paper, we increase the vertical resolution so that it will be comparable with the horizontal resolution. Cold fronts have a typical slope of 50 to 1 so we should have $\Delta x/\Delta z\approx 50$. Since the minimum value of Δx that we can consider is 50 km, we choose $\Delta z=1$ km.

Consequently, for all our numerical calculations, we take

$$K=9, \quad z_k-z_{k-1}=1\text{ km}.$$

Unauthenticated | Downloaded 10/14/24 09:06 AM UTC

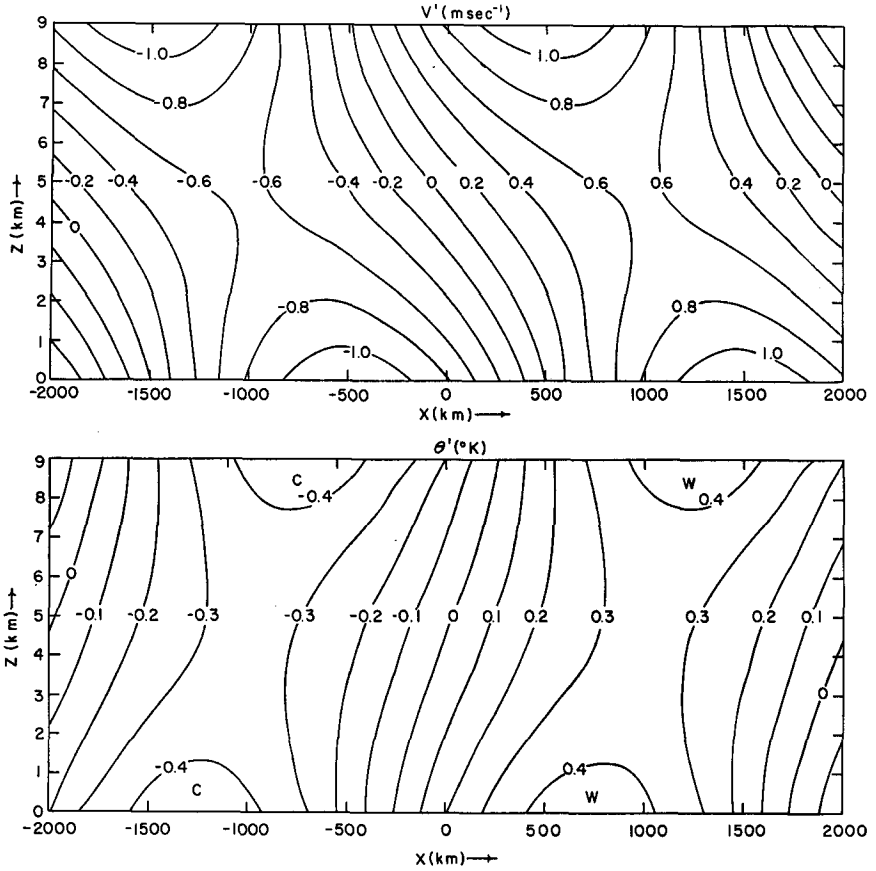

FIG. 2. The initial fields for experiment 1a as functions of x and z. Top, $v'=v-\bar{v}$; bottom, $\theta'=\theta-\bar{\theta}$. The bar represents the horizontal average.

In experiment 1a we take

$$\Delta x=200 \text{ km}, \quad \Delta t=30 \text{ min},$$

while we will use a smaller grid size in experiment 1b.

In order to interpret the initial evolution of the numerical solution, let us compute the nondimensional numbers which appear in Eqs. (4.4)–(4.6). We find that Ro=0.221 and this value is invariant in time. The disturbance Rossby number $\mathfrak{R}$o has the value 0.016. This value is obtained by taking V equal to the maximum value of v along the lowest level in the domain (z=0.5 km). The other numbers are $b=1$, $a\sim O(1)$, and $\Gamma\sim O(1)$. The numbers $\mathfrak{R}$o, a and b change as the disturbance changes, but Γ remains of order 1.

Initially, $\mathfrak{R}$o and Ro^2 are very small so we may neglect them in Eqs. (4.4)–(4.6). The resulting system of equations is the quasi-geostrophic set (see W2L). Thus, the early evolution of the numerical solution should be very close to the quasi-geostrophic solution. The unstable quasi-geostrophic solutions for our initial basic state were obtained by Eady (1949), and the general quasi-geostrophic solution was obtained by Pedlosky (1964). Exponential instability occurs when the wave number $1/L$ is smaller than (1.09) $(f/D)[(\theta_0/g)\partial\bar{\theta}_I/\partial z]^{\frac{1}{2}}$.

The wavelength of our initial disturbance was selected to give the maximum growth rate, and the structure of the initial disturbance is that of the exponentially growing eigensolution. If a more general initial state were used, this exponentially growing mode would eventually predominate provided that the initial amplitude were sufficiently small.

With these initial conditions, the initial disturbance will grow exponentially without changing its structure until the disturbance amplitude becomes large. Thus, the disturbance Rossby number will grow and when it reaches a finite value, the nonlinear terms in Eqs. (4.4) and (4.6) will cause distortions in the quasi-geostrophic solutions. These distortions take the form of a cold frontal zone.

The time variation of the disturbance is shown in Fig. 3 at z=0.5 km; the distortions in the disturbance are largest at this level. At each time, $u'=u-\bar{u}$, $v'=v-\bar{v}$, and $\theta'=\theta-\bar{\theta}$ are plotted as functions of x on different scales. The following table gives $\mathfrak{R}$o and b for

	t=0	t=4	t=5	t=5.5
$\mathfrak{R}_0$	0.016	0.5	1.82	4.05
b	1.0	0.7	0.4	0.34

Unauthenticated | Downloaded 10/14/24 09:06 AM UTC

the times t (in days) given in Fig. 3. We have taken $\mathcal{R}o$ as equal to the maximum value of $\partial v/\partial x$ divided by f. The table shows that horizontal scale decreases as $\mathcal{R}o$ increases since b is the ratio of the scale to the initial scale. This change of scale is evident in Fig. 3. At each time we note that the horizontal convergence $(-\partial u/\partial x)$ is correlated with the vorticity $(\partial v/\partial x)$. We shall see that this correlation is crucial in the development of the frontal zone. At $t=5$ days the region of maximum vorticity near $x=500$ km clearly represents a cold front. Although the temperature field also suggests a warm front, the vorticity field does not. The presence of large distortions in the various fields at this time is consistent with the importance of the nonlinear terms in Eqs. (4.4) and (4.6). Eq. (4.5) predicts that the v component will still be geostrophic at this time, and we shall see that this is actually the case. At $t=5.5$ days the scale of the frontal zone is quite small, and some spurious oscillations are present which are a result of the truncation error.

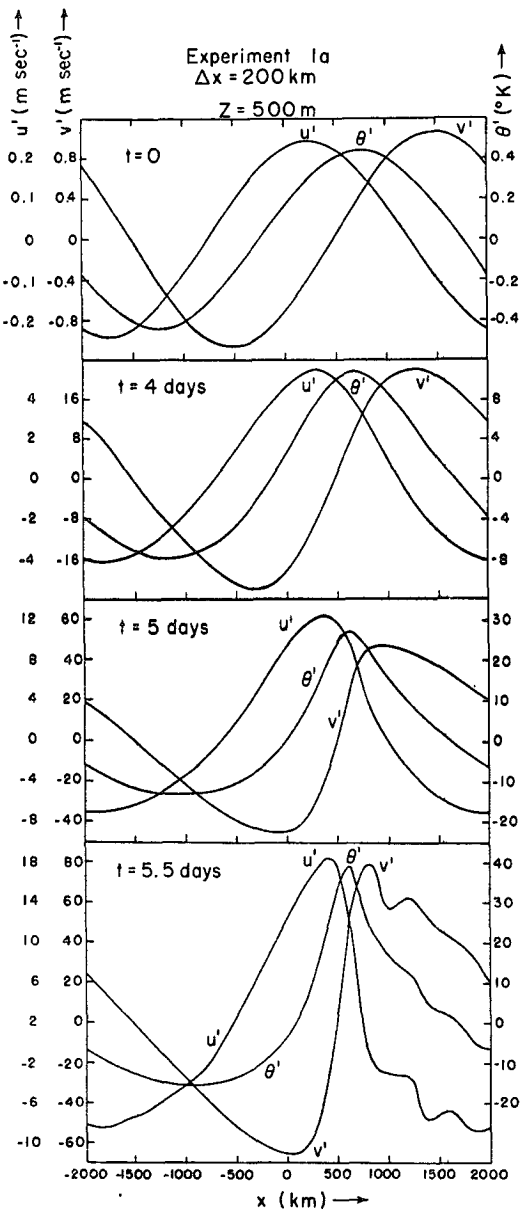

FIG. 3. The fields at $z=0.5$ km from experiment 1a for various times, $t=0$, 4, 5 and 5.5 days.

Since the scale of the front at $t=5.5$ days is near the grid size, a further reduction in the scale of the front will be greatly restricted. In fact, the front cannot have a scale which is less than Δx. If we are to study the frontogenesis process further, we must reduce the grid size.

In experiment 1b we choose $\Delta x=50$ km and $\Delta t=7.5$ min. Rather than go back to $t=0$ with the new grid, we use the solution from experiment 1a at $t=3$ days; at this time the truncation error should be very small. For simplicity, we use only wave numbers 1 and 2 of experiment 1a as initial conditions for experiment 1b because they describe more than 99% of the solution at $t=3$ days.

Fig. 4a contains the v field at $t=5$ days for both experiments, and it can be seen that the frontal zone is narrower in the experiment with the smaller grid size. This indicates that the truncation error in experiment 1a is already inhibiting the energy transfer to the short waves. In Fig. 4b we have $v-\bar{v}$, $u-\bar{u}$, and $\theta-\bar{\theta}$ at $t=5.5$ days in experiment 1b. If we look at the v field, for example, we note that the frontal width is already of the order of Δx; this was also the case in experiment 1a. This suggests that for $t\approx 5.5$ days, the frontal width, in general, would be of the order of Δx. If this were the case, the exact solution to the continuous equations would become discontinuous at about this time. This result strongly implies that the vertical deformation field can produce a realistic front within a finite period of time.

The time variation of the scale of the frontal zone at $z=0.5$ km is presented in Fig. 5 for both experiments. The width of the frontal zone is computed from the expression,

$$W=2l=\frac{v_{\max}-v_{\min}}{(\partial v/\partial x)_{\max}}. \tag{6.1}$$

In experiment 1a the change in scale during the first 3 days is small because the solution is essentially the exponentially growing geostrophic mode which has a fixed structure. After $t=3$ days the scales in both experiments begin to decrease rapidly. Except for near its inception, the $\Delta x=50$ km (experiment 1b) curve always shows a smaller scale than the $\Delta x=200$ km (experiment 1a) curve. During the period from 3 to 5.5 days, the scales in both experiments decrease almost linearly, and thereafter they oscillate about values near $2\Delta x$. As noted before, W cannot be less than Δx. If the curve for experiment 1b were extrapolated linearly beyond 5.5 days, a discontinuity would occur within a

Unauthenticated | Downloaded 10/14/24 09:06 AM UTC

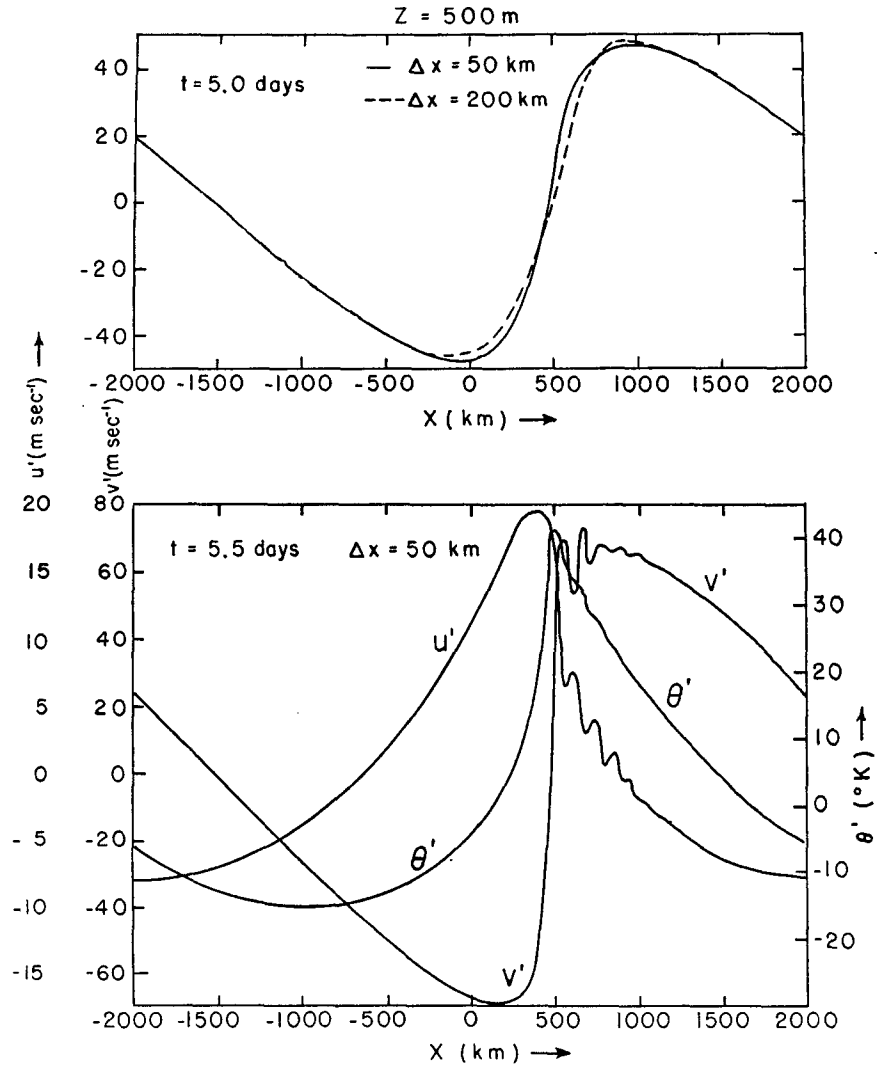

FIG. 4. The fields at $z=0.5$ km. Top, v' from both experiments at $t=5$ days; bottom, u', v' and θ' from experiment 1b at $t=5.5$ days. In experiments 1a and 1b, Δx equals 200 km and 50 km, respectively.

few hours. This again indicates that a discontinuity in the tangential wind component would occur if the truncation error could be eliminated.

Fig. 6 shows the Fourier amplitudes of v at $z=0.5$ km in experiment 1b during the period from $t=3$ to $t=6$ days. The wave number is m, and $m=1$ corresponds to the wave which is initially unstable. Up to 5.5 days the curves are nearly linear, indicating that all components are growing exponentially (the scale is logarithmic). In W2L finite amplitude perturbation solutions were obtained which behave in this manner. It was predicted that if n were the growth rate of wave number 1, than the growth rate of wave number m would be mn. This relation is approximately satisfied for the solutions in Fig. 6. These harmonics are in phase with each other in such a way that they produce a large gradient in the frontal zone.

It was suggested above that the v field would reach a finite jump in x if the truncation error could be eliminated. This situation can be described roughly by the saw-tooth function,

$$F(x)=\begin{cases}-\dfrac{\pi}{2}-x, & -\dfrac{\pi}{2}\leq x<0\\[2ex] \dfrac{\pi}{2}-x, & 0<x\leq\dfrac{\pi}{2}.\end{cases} \tag{6.2}$$

The Fourier amplitudes of $F(x)$ vary in proportion to $1/m$, if m is the wave number. Fig. 7 displays the Fourier amplitudes for v at $t=5.5$ days on a log-log plot. This spectrum is for the field at $z=0.5$ km from experiment 1b. The major portion of the spectrum obeys a power law with an exponent of -1.27. Thus, the v

Unauthenticated | Downloaded 10/14/24 09:06 AM UTC

spectrum is approaching the $1/m$ behavior of the sawtooth function. The rapid growth of the short waves shown in Fig. 6 is necessary if a $1/m$ spectrum is to be produced from an initial spectrum which contains only wave number 1. This energy cascade arises entirely from the non-geostrophic advections since the quasi-geostrophic equations for this model are linear and thus cannot change the scale of the disturbance.

Let us now examine the vertical structure of the frontal zone. Fig. 8 shows $v'=v-\bar{v}$ and $\theta'=\theta-\bar{\theta}$ from experiment 1b at $t=5$ days. The v field is similar in general form to the initial v field (Fig. 2). However, the gradients in the cyclonic region are much larger than in the anticyclonic region; initially, the gradients were of equal magnitude in both regions. The cold frontal zone, which is indicated by the zone of maximum cyclonic shear, is most intense at the surface and at the upper boundary. This frontal zone is most diffuse in the center of the region where $z=4.5$ km. The cold frontal zone tilts westward with height, and there is no indication of a warm front which would tilt eastward with height in the vorticity field.

The lower portion of Fig. 8 contains the perturbation potential temperature. In the cold frontal zone, we note that the region of maximum horizontal temperature gradient shows a westward tilt with height. But the θ' field shows practically no vertical tilt with height in the frontal zone. Intense atmospheric fronts are normally quite stable in the sense that there is a large increase in θ' as one passes up through the front. But our numerical solution is approaching such a state because the initial

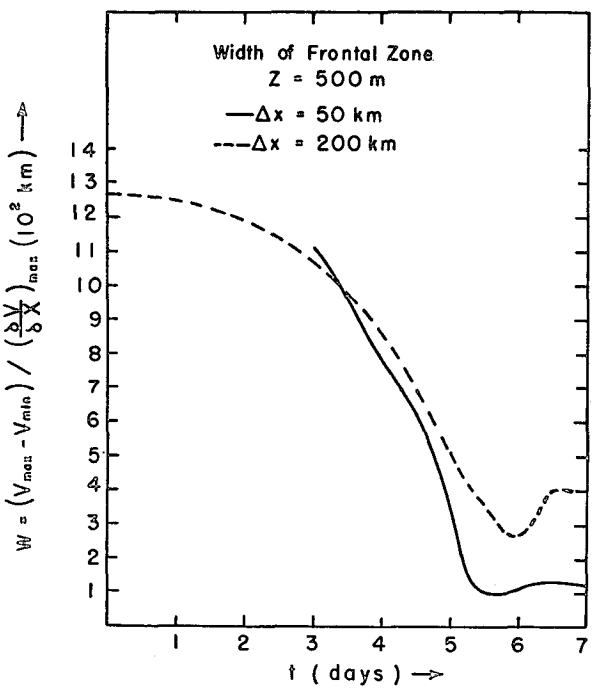

FIG. 5. The time variation of the frontal scale at $z=0.5$ km for the two experiments.

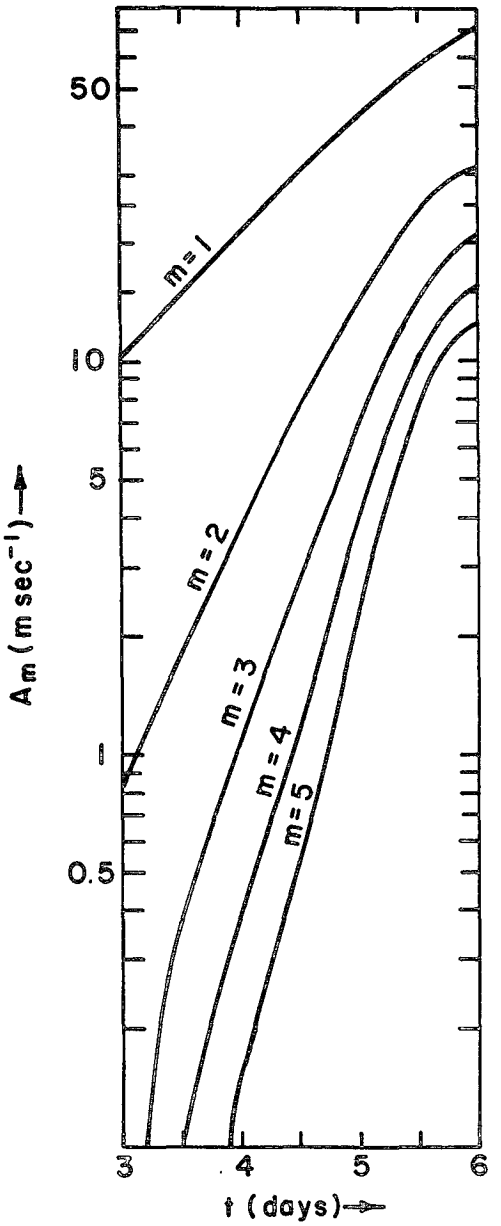

FIG. 6. The Fourier amplitudes of v on a logarithmic scale at $z=0.5$ km in experiment 1b. The amplitude is defined from $v=\sum_m A_m \cos\{m[(x/L)-\delta_m)]\}$.

disturbance actually contained a vertical decrease in θ' in what was to become the cold frontal zone (Fig. 2). As was the case with v, the largest gradients in θ are found near the two boundaries. Although no warm front is discernible, the occlusion process is occurring since the region of warm air occupies a smaller area at the lower surface than it does at the upper surface.

The symmetry which is defined by Eq. (5.7) is clearly present in the fields which are shown in Fig. 8 as was predicted earlier. Consequently, we give only the lower half domain ($0\leq z\leq 4.5$ km) in Fig. 9. In this figure, u', v' and Ψ' are shown at $t=5.5$ days from experiment 1b.

Unauthenticated | Downloaded 10/14/24 09:06 AM UTC

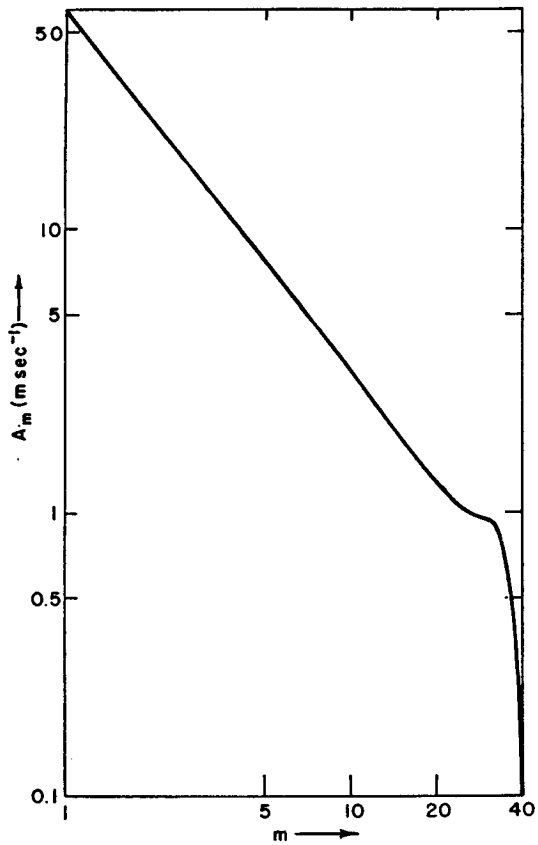

FIG. 7. The Fourier amplitudes of v on a logarithmic scale plotted against the logarithm of the wave number at $t=5.5$ days from experiment 1b.

The stream function $\bar{\Psi}$ is defined as

$$u=\partial\bar{\Psi}/\partial z, \quad w=-\partial\bar{\Psi}/\partial x. \tag{6.3}$$

The stream function satisfies the even symmetry condition, $\bar{\Psi}(x, z-D/2)=\bar{\Psi}(-x, -z+D/2)$. In Fig. 9a we note that the width of the frontal zone at the surface is much less than it is in the interior. In fact, the frontal thickness at $z=0$ is about 100 km as compared to 570 km at $z=4.5$ km. At this time the difference between the cyclonic region and the anticyclonic is even more marked than it was at $t=5$ days. The θ' field also contains larger gradients than it did at $t=5$ days, and a small vertical increase in θ' is now present in the frontal zone. The $\bar{\Psi}$ field, which represents the circulation in the x-z plane, is composed of two cells. The more intense of the two represents a thermally direct circulation about the cold frontal zone. It can be seen that horizontal convergence is occurring at the location of the surface front.

The time changes in the zonally averaged fields of experiments 1a and 1b are very similar to those obtained in W2L. That is, $\bar{u}$ becomes greater than the geostrophic wind, $\bar{v}$ becomes positive, and $\bar{\theta}$ becomes greater than $\bar{\theta}_I$ in the upper half of the domain. These fields will not be shown because they do not play an important role in the frontogenesis process.

As a measure of the computational error in the total energy, we define

$$e=\frac{E-E_0}{(\overline{u^2}+\overline{v^2})/2}, \tag{6.4}$$

where E is given by Eq. (2.21). In experiment 1b, E_0 is the value of E at $t=3$ days. For $t\leq 6$ days in this experiment e remained below 0.5×10^{-4}. Thus, over the period of interest the error in the total energy is negligible.

7. Simplified analytical model

In this section, we shall construct a crude analytical model which gives the same gross behavior as was obtained numerically in Section 6. However, this model is not good enough to permit qualitative comparisons.

The nonlinear advections which produce the front depend on the circulation in the x-z plane. We can derive a diagnostic equation for the stream function in this plane under certain conditions. If we eliminate v^* and ϕ^* from Eq. (4.5) with Eqs. (4.4), (4.6) and (4.8), we obtain

$$\left(\frac{\partial^2}{\partial z^{*2}}+\Gamma\frac{\partial^2}{\partial x^{*2}}\right)\psi+\mathfrak{Ro}\left[\frac{\partial}{\partial z^*}\left(\frac{\partial\psi}{\partial z^*}\frac{\partial v^*}{\partial x^*}-\frac{\partial\psi}{\partial x^*}\frac{\partial v^*}{\partial z^*}\right)-\frac{\partial}{\partial x^*}\left(\frac{\partial\psi}{\partial z^*}\frac{\partial\theta^*}{\partial x^*}-\frac{\partial\psi}{\partial x^*}\frac{\partial\theta^*}{\partial z^*}\right)\right]$$
$$+\frac{\mathrm{Ro}^2}{b^2}\left\{\left[\frac{\partial}{\partial t^*}+(2az^*-1)\frac{\partial}{\partial x^*}\right]\frac{\partial}{\partial z^*}\left[\frac{\partial^2\psi}{\partial z^*\partial t^*}+(2az^*-1)\frac{\partial^2\psi}{\partial x^*\partial z^*}-2a\frac{\partial\psi}{\partial x^*}\right.\right.$$
$$\left.\left.+b\mathfrak{Ro}\left(\frac{\partial\psi}{\partial z^*}\frac{\partial^2\psi}{\partial x^*\partial z^*}-\frac{\partial\psi}{\partial x^*}\frac{\partial^2\psi}{\partial z^{*2}}\right)\right]\right\}=-\frac{4a}{b}\frac{\partial v^*}{\partial x^*}, \tag{7.1}$$

where $\partial\psi/\partial x^*=-w^*$, $\partial\psi/\partial z^*=u^*$.

This equation reduces to the quasi-geostrophic omega equation when the terms in Ro and $\mathfrak{Ro}$ are neglected (to obtain the precise form, we must also differentiate with respect to x^*). If we neglect only the terms in Ro^2, we obtain the equation which Eliassen (1962) derived in a study of frontal circulations. We shall call this the balance approximation since it can be obtained di-

Unauthenticated | Downloaded 10/14/24 09:06 AM UTC

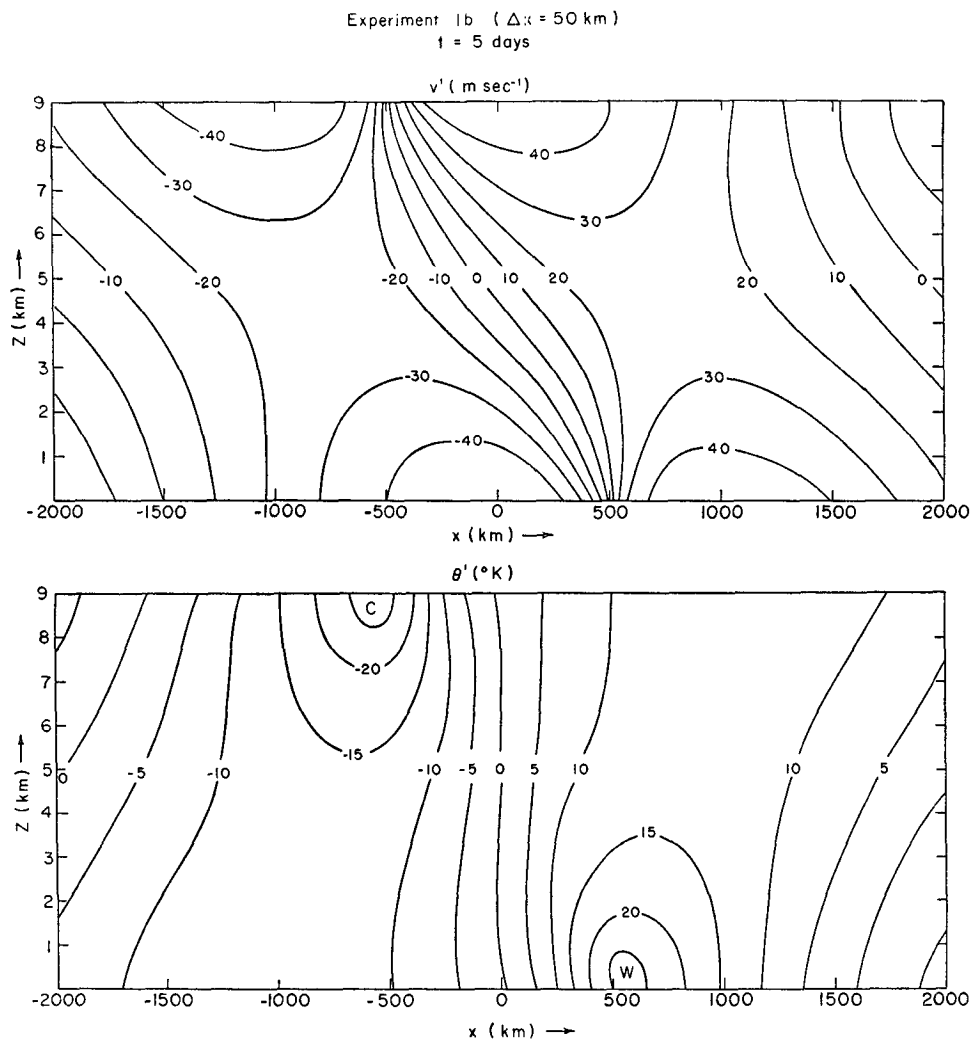

FIG. 8. The fields at $t=5$ days for experiment 1b as functions of x and z. Top, $v'=v-\bar{v}$; bottom, $\theta'=\theta-\bar{\theta}$.

rectly from the "balance equations" (Charney, 1962). The scale analysis implies that this approximation will be good as long as $\mathrm{Ro}^2\mathcal{R}\mathrm{o}/b\ll 1$, provided that $a/b\sim O(1)$. The latter is satisfied as long as the frontal slope ℓ/d is of the order of 100, and this is the case in our numerical integrations. The ratio $\mathcal{R}\mathrm{o}/b$ can become rather large without violating our condition since $\mathrm{Ro}^2=0.05$. The neglect of the Ro^2 term implies that the v component is geostrophic [Eq. (4.5)].

Fig. 10 shows v' and $v_g=f^{-1}\partial\phi/\partial x$ at $t=5.5$ days and $z=0.5$ km in experiment 1b. Since the maximum difference is only about 10%, the balance approximation should be accurate up to this time. It is possible that the difference between v and v_g would become large when $\mathcal{R}\mathrm{o}/b$ is very large, but we cannot answer this question from our numerical solutions.

Thus, the numerical integrations justify the scaling used for u and they indicate that the balance approximation is valid throughout most of the frontogenesis process. If we use the geostrophic relation, $\partial v^*/\partial z^* = \partial\theta^*/\partial x^*$, we can write the balance approximation in the form:

$$\left[1+\mathcal{R}\mathrm{o}\frac{\partial v^*}{\partial x^*}\right]\frac{\partial^2\psi}{\partial z^{*2}}-2\mathcal{R}\mathrm{o}\frac{\partial v^*}{\partial z^*}\frac{\partial^2\psi}{\partial x^*\partial z^*}+\left[\Gamma+\mathcal{R}\mathrm{o}\frac{\partial\theta^*}{\partial z^*}\right]\frac{\partial^2\psi}{\partial x^{*2}}=-\frac{4a}{b}\frac{\partial v^*}{\partial x^*}. \quad (7.2)$$

This equation is elliptic provided that

$$(1+\mathcal{R}\mathrm{o}\,\partial v^*/\partial x^*)\left[\Gamma+\mathcal{R}\mathrm{o}\frac{\partial\theta^*}{\partial z^*}\right]-\mathcal{R}\mathrm{o}^2(\partial v^*/\partial z^*)^2>0.$$

If this condition is satisfied, (7.2) can be solved for ψ if θ^* and v^* are prescribed and if appropriate boundary conditions are given for ψ. This is not easy to do analytically unless $\mathcal{R}\mathrm{o}$ can be neglected since the co-

Unauthenticated | Downloaded 10/14/24 09:06 AM UTC

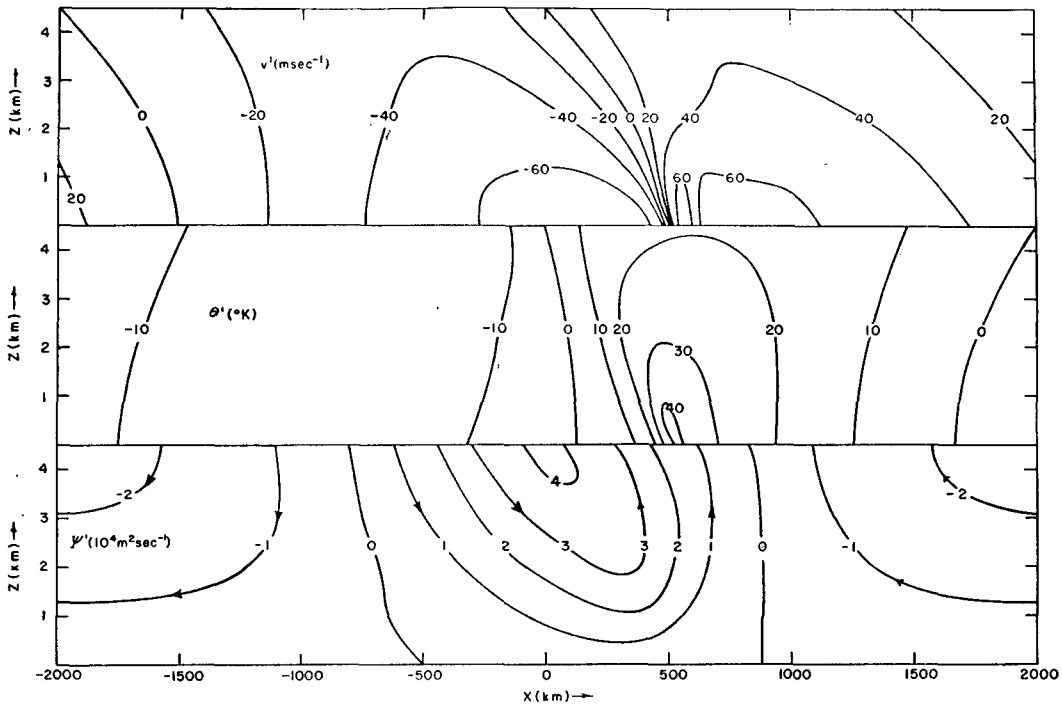

FIG. 9. The fields at $t=5.5$ days for experiment 1b in the lower half of the domain. Top, $v'=v-\bar{v}$; middle, $\theta'=\theta-\bar{\theta}$; bottom, $\Psi'=\Psi-\bar{\Psi}$.

efficients will generally be functions of x^* and z^*. Later in this section we will solve (7.2) by making a boundary layer type assumption.

Since v is approximately geostrophic, we can find the time evolution of θ if we know the evolution of v. Thus, if we can show that v will develop a frontal character, θ will also have one. The dimensional vorticity equation is

$$\frac{\partial}{\partial t}\left(\frac{\partial v}{\partial x}\right)=-u\frac{\partial}{\partial x}\left(\frac{\partial v}{\partial x}\right)-w\frac{\partial}{\partial z}\left(\frac{\partial v}{\partial x}\right)$$
$$-(f+\partial v/\partial x)(\partial u/\partial x)-(\partial w/\partial x)(\partial v/\partial z). \quad (7.3)$$

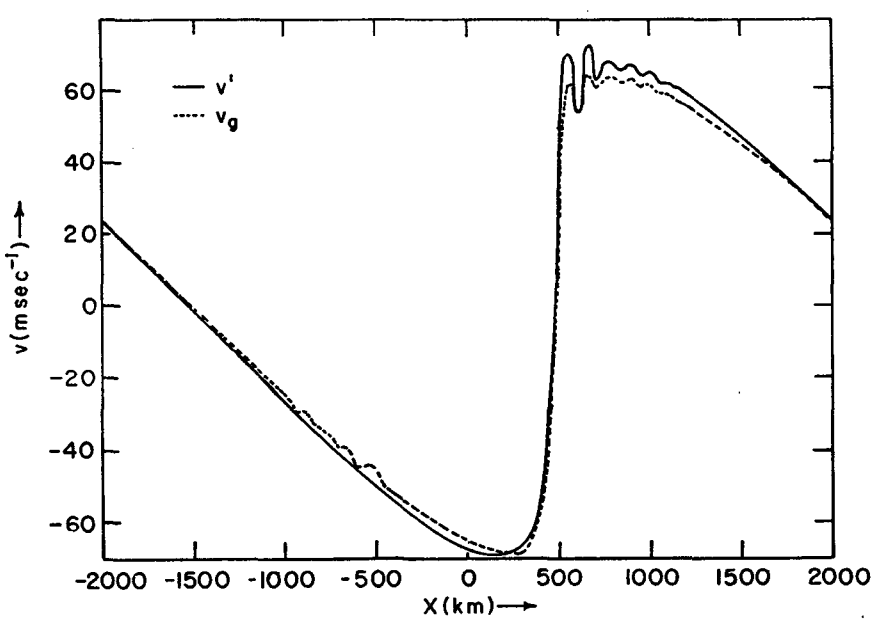

FIG. 10. The fields v' and $v_g=f^{-1}(\partial\phi/\partial x)$ at $t=5.5$ days and $z=0.5$ km in experiment 1b.

Unauthenticated | Downloaded 10/14/24 09:06 AM UTC

In order to find the evolution of the disturbance, one can make a perturbation expansion in the disturbance amplitude as was done in W2L. However, these solutions are not valid when $\mathcal{R}o$ becomes of order 1 or larger. We can study the large amplitude portion of the evolution if we assume that a frontal zone is present and then ask if it will intensify.

Applying Eq. (7.3) at $z=0$ where the frontogenesis is a maximum, we obtain

$$\frac{\partial}{\partial t}\left(\frac{\partial v}{\partial x}\right)=-u\frac{\partial}{\partial x}\left(\frac{\partial v}{\partial x}\right)-\left(f+\frac{\partial v}{\partial x}\right)\frac{\partial u}{\partial x}. \tag{7.4}$$

Suppose that the vorticity is a maximum at $x=x_f$; this is the point where the front intersects the ground. Because our frame of reference moves with the mean flow, x_f is approximately constant during the frontogenesis process as can be seen from the figures in Section 6. Thus, we assume that

$$\frac{\partial x_f}{\partial t}=0, \tag{7.5}$$

and can then write (7.4) at $x=x_f$ in the form

$$\frac{d}{dt}\left(\frac{\partial v}{\partial x}\right)=-\left(f+\frac{\partial v}{\partial x}\right)\frac{\partial u}{\partial x}, \tag{7.6}$$

where $d/dt=(\partial/\partial t)_{x=x_f}$.

We can solve (7.6) if we can find a relation between $\partial v/\partial x$ and $\partial u/\partial x$; this relation can be obtained from Eq. (7.2).

First we define the following coordinate system which is imbedded in the frontal zone:

$$\xi=s(\alpha x^*-z^*), \quad \zeta=s(x^*+\alpha z^*), \tag{7.7}$$

where $s=(1+\alpha^2)^{-\frac{1}{2}}$.

We shall neglect the curvature of the frontal surface in this simple analysis. The frontal surface is given by $\zeta=$constant, and the frontal slope is $\alpha=-(dx^*/dz^*)_f$. Now we make the boundary layer assumption that the variations normal to the front are much larger than the variations along the front. Thus, if χ is ψ, v^* or θ^*, the condition is

$$\left|\frac{\partial \chi}{\partial \zeta}\right|\gg\left|\frac{\partial \chi}{\partial \xi}\right|. \tag{7.8}$$

If we now introduce the new coordinates (7.7) into Eq. (7.2) and use the approximation (7.8) we obtain

$$\frac{\partial^2\psi}{\partial\zeta^2}=-\frac{4a}{b}\frac{\partial v^*/\partial\zeta}{s[\alpha^2+\Gamma]}, \tag{7.9}$$

where we also used the geostrophic relation, $\partial\theta^*/\partial\zeta=\alpha\partial v^*/\partial\zeta$. Note that this equation is independent of $\mathcal{R}o$. The vorticity and the divergence in this coordinate system are

$$\frac{\partial v^*}{\partial x^*}=s\frac{\partial v^*}{\partial\zeta}, \quad \frac{\partial u^*}{\partial x^*}=s^2\alpha\frac{\partial^2\psi}{\partial\zeta^2}. \tag{7.10}$$

If we use these in (7.9) and return to dimensional quantities, we obtain

$$\frac{\partial u}{\partial x}=-\frac{4l\alpha U\,\partial v/\partial x}{Ddf[(l^2\alpha^2/d^2)+(g/\theta_0)f^{-2}d\bar{\theta}_I/dz]}. \tag{7.11}$$

A relation similar to this was derived by Sawyer (1952) in a study of the vertical motion change across a front.

We can now solve Eq. (7.6) if we apply Eq. (7.11) at $z=0$. However, Eq. (7.11) may not be valid at the surface since we have assumed that the principle variation of ψ is normal to the front. This cannot be the case at $z=0$ because ψ must be constant there. We shall nevertheless use (7.11) because it should be at least qualitatively correct at the surface.

The required substitution of (7.11) into (7.6) yields

$$\frac{d}{dt}\left(\frac{\partial v}{\partial x}\right)-N[1+(1/f)(\partial v/\partial x)](\partial v/\partial x)=0, \tag{7.12}$$

where

$$N=\frac{4l\alpha U}{Dd[(l^2\alpha^2/d^2)+(g/\bar{\theta}_0)f^{-2}d\bar{\theta}_I/dz]}.$$

The solution is

$$\frac{\partial v}{\partial x}=\frac{(\partial v/\partial x)_0 e^{Nt}}{1-(1/f)(\partial v/\partial x)_0(e^{Nt}-1)}, \tag{7.13}$$

where $(\partial v/\partial x)_0$ is the initial vorticity. If the initial Rossby number, $(1/f)(\partial v/\partial x)_0$, is small, the solution will grow exponentially until the second term in the denominator becomes important. This corresponds to the first portion of our numerical solution in which the disturbance grows exponentially without changing its shape. In the frontal situation where $(\partial v/\partial x)_0>0$, the denominator will decrease with time and it will reach zero when $t=t_f$, where

$$t_f=\frac{1}{N}\log[1+f/(\partial v/\partial x)_0]. \tag{7.14}$$

At this time the vorticity will become infinite and, since v must be bounded, this implies that a frontal discontinuity will occur. For t close to t_f, the scale of the front will decrease linearly as was found for the numerical solutions (Fig. 5). This very crude model predicts qualitatively the development of the front at the surface.

In order to interpret this process physically, we return to the vorticity equation (7.4). Only the divergence term can increase the maximum vorticity and only the

Unauthenticated | Downloaded 10/14/24 09:06 AM UTC

nonlinear portion of it can change the scale of v. In the linear portion of the evolution, the divergence must be negative at the point of maximum vorticity because otherwise the disturbance could not grow. Eq. (7.2) states that the strength of the divergent circulation is proportional to the vorticity. If the negative correlation between $\partial u/\partial x$ and $\partial v/\partial x$ is maintained, the nonlinear term will cause the vorticity to grow at an increasing rate, and this will continue until the vorticity becomes singular within a finite period of time. Both the simple theory and the numerical solutions show that this negative correlation is maintained. Physically, the convergence field at the front brings air parcels with northward momentum from ahead of the front adjacent to parcels with southward momentum from behind the front in a finite time, and this produces an infinite shear.

The general vorticity equation (7.3) determines the evolution of the front away from the two horizontal boundaries. The last two terms should be dominant at the front since the other terms represent advections. We can expect that $\partial v/\partial x$ and $\partial u/\partial x$ will be negatively correlated at all heights [Eq. (7.11)]. The twisting term, $-(\partial w/\partial x)(\partial v/\partial z)$, will be negative at the front because there is rising motion ahead of the front and sinking motion behind it and because v increases up through the front (Fig. 9). Thus, as one moves away from the boundary, the magnitude of the twisting term increases and the frontogenesis decreases. This is shown clearly in Figs. 8 and 9 for both v' and θ'. If we compute the twisting from (7.9), we obtain

$$[(\partial v/\partial x)(\partial u/\partial x)+(\partial w/\partial x)(\partial v/\partial z)]=0. \quad (7.15)$$

Thus, there can be no frontogenesis in the context of this simple model when the boundaries are far enough away that the twisting term assumes its full value. This shows the crucial role which the boundaries play in frontogenesis.

8. Conclusion and suggestions for further studies

We have shown numerically that a growing baroclinic wave can distort itself through the divergent advections which are associated with the vertical deformation fields in such a manner that a realistic cold frontal zone is produced. The comparison of the solutions for different values of Δx indicates that the width of the frontal zone would attain zero in a finite time in the absence of numerical errors. The advection terms which produce the distortions are of the order of the disturbance Rossby number which is normally small for large scale flow. In our example the Rossby number grows to a finite amplitude as a result of the growth of the baroclinic wave. The amplitude of the v component in our experiments becomes larger than 50 m sec^{-1} before the front forms and this is much larger than is typical in the atmosphere. However, since it is the Rossby number that is important, the atmosphere can produce fronts by starting with a smaller spacial scale; in that case, such large velocities would not be required.

The crude analytical solution, which was obtained in Section 7, gives the gross behavior of the front at the surface and it predicts that v will become discontinuous within a finite period of time. When $\partial v/\partial x \gg f$, Eq. (7.12) takes the same form as the equation which describes the development of a shock or a pressure jump (Platzman, 1964). Physically, the formation of the front is quite different from the formation of a shock or a pressure jump because the frontal case is rotationally dominated, i.e., $|\partial v/\partial x| \gg |\partial u/\partial x|$.

Many more cases must be examined before a general theory of atmospheric frontogenesis can be solidified. We hypothesize that frontogenesis normally occurs in the following manner. First, quasi-geostrophic processes cause the Rossby number to reach a finite value in certain regions. This could be accomplished through baroclinic instability or through the process considered by Stone (1966). When the Rossby number becomes sufficiently large, the vertical deformation field would rapidly reduce the frontal scale to zero or to a limiting frictional value. Once the Rossby number becomes large, this process would be much more efficient than the one described by Stone since his shows only an exponential decrease in the scale.

It would be very useful if a more satisfactory analytical solution describing the frontogenesis process could be derived. A boundary layer procedure is probably required, but the location and structure of the boundary layer must be functions of time.

Friction is probably the most important effect which we have neglected. In particular, the vertical diffusion of momentum near the surface should be important when the surface velocities are large. In general, turbulent mixing must determine the ultimate frontal scale. Other important effects which were neglected are the latent heat of condensation, the compressibility of the air, and the variation of f with latitude. The latent heat of condensation is the only one of these which is difficult to include in the calculations.

The initial conditions which we used render the variation of the disturbance in one direction (y) unimportant, and this is also true of Stone's work. This can be justified, in general, once the front becomes sufficiently intense that the normal gradients predominate. However, in typical atmospheric disturbances, both horizontal dimensions are important. Thus, it is very important to understand how such a disturbance can evolve into one in which one direction dominates. One example of this process was obtained numerically by Edelmann (1963).

The characteristics of our frontal model must be compared with observations. The most important features to be compared are the time scale of formation and the frontogenesis mechanism. Our time scale is less than 24 hr if we count from a time when the disturbance amplitude is large. Plotkin (1965) gives an example in which a diffuse front is transformed into an

Unauthenticated | Downloaded 10/14/24 09:06 AM UTC

intense one during a period of much less than 24 hr. Sanders (1955) and Plotkin found intense convergence at the surface frontal position. Sanders also found that the width of the frontal zone increased rapidly with height as a result of the twisting effect. Their analyses are thus consistent with our numerical solutions. There is great need for more careful analyses of actual examples of frontogenesis.

Acknowledgments. The author wishes to thank Profs. J. G. Charney and N. A. Phillips for several stimulating discussions on the frontogenesis problem. The author also wishes to thank Prof. S.-K. Kao for reading the manuscript and for making useful comments upon it. The manuscript was carefully typed by Mrs. Drue Ross. This research was supported by the National Science Foundation under Grant G-18985 at the Massachusetts Institute of Technology.

REFERENCES

Arakawa, A., 1962: Non-geostrophic effects in the baroclinic prognostic equations. *Proc. Intern. Symp. Numerical Weather Prediction*, Tokyo, 161–175.

——, 1966: Computational design for long-term numerical integration of the equations of fluid motion: Two-dimensional incompressible flow. Part I. *J. Comput. Phys.*, **1**, 119–143.

Bergeron, T., 1928: Über die dreidimensional verknüpfende Wettranalyse I. *Geofys. Publikasjoner*, **5**, No. 6, 1–111.

Charney, J. G., 1962: Integration of the primitive and balance equations. *Proc. Intern. Symp. Numerical Weather Prediction*, Tokyo, 131–152.

——, and M. Stern, 1962: On the stability of internal baroclinic jets in a rotating atmosphere. *J. Atmos. Sci.*, **19**, 159–172.

Eady, E. T., 1949: Long waves and cyclone waves. *Tellus*, **1**, No. 3, 33–52.

Edlemann, W., 1963: On the behavior of disturbances in a baroclinic channel. Sum. Rept. No. 2, Research in Objective Weather Forecasting, Part F, Contract No. AF 61(052)-373, Research Division, Deutscher Wetterdienst, Offenbach, 35 pp.

Eliassen, A., 1959: On the formation of fronts in the atmosphere. *The Atmosphere and the Sea in Motion*, New York, Rockefeller Institute Press and the Oxford University Press, 277–287.

——, 1962: On the vertical circulation in frontal zones. *Geofys. Publikasjoner*, **24**, No. 4, 147–160.

Fallier, A. J., 1956: A demonstration of fronts and frontal waves in atmospheric models. *J. Meteor.*, **13**, 1–4.

Hinkelmann, K., 1959: Ein numerisches Experiment mit den primitiven Gleichungen. *The Atmosphere and the Sea in Motion*, New York, Rockefeller Institute Press and the Oxford University Press, 486–500.

Knauss, J. A., 1957: An observation of an oceanic front. *Tellus*, **9**, 234–237.

Lamb, H., 1945: *Hydrodynamics*. New York, Dover Publications, 738 pp.

Lilly, D. K., 1965: On the computational stability of numerical solutions of time-dependent non-linear geophysical fluid dynamics problems. *Mon. Wea. Rev.*, **93**, 11–26.

Lorenz, E. N., 1960: Energy and numerical weather prediction. *Tellus*, **12**, 364–373.

Ogura, Y., and N. A. Phillips, 1962: Scale analysis of deep and shallow convection in the atmosphere. *J. Atmos. Sci.*, **19**, 173–179.

Pedlosky, J., 1964: An initial value problem in the theory of baroclinic instability. *Tellus*, **16**, 12–17.

Phillips, N. A., 1959: An example of nonlinear computational instability. *The Atmosphere and the Sea in Motion*, New York, Rockefeller Institute Press and the Oxford University Press, 501–504.

——, 1963: Geostrophic motion. *Rev. Geophys.*, **1**, 123–176.

Platzman, G. W., 1964: An exact integral of complete spectral equations for unsteady one-dimensional flow. *Tellus*, **16**, 422–431.

Plotkin, J., 1965: Detailed analysis of an intense surface cold front. M. S. Thesis, Massachusetts Institute of Technology, 42 pp.

Sanders, F., 1955: Investigation of the structure and dynamics of an intense surface frontal zone. *J. Meteor.*, **12**, 542–552.

Sawyer, J. S., 1952: Dynamical aspects of some simple frontal models. *Quart. J. Roy. Meteor. Soc.*, **78**, 170–178.

Smagorinsky, J., 1958: On the numerical integration of the primitive equations of motion for baroclinic flow in a closed region. *Mon. Wea. Rev.*, **86**, 457–466.

Stone, P. H., 1966: Frontogenesis by horizontal wind deformation fields. *J. Atmos. Sci.*, **23**, 455–465.

Williams, R. T., 1965: Nonlinear, non-geostrophic effects in a baroclinic atmosphere. *J. Atmos. Sci.*, **22**, 388–401.

Unauthenticated | Downloaded 10/14/24 09:06 AM UTC